

Article

Methanation of Carbon Dioxide over Ni–Ce–Zr Oxides Prepared by One-Pot Hydrolysis of Metal Nitrates with Ammonium Carbonate

Wangxin Nie ^{1,2}, Xiuqing Zou ^{1,2,*}, Chenju Chen ^{1,2}, Xueguang Wang ^{1,2,*}, Weizhong Ding ^{1,2} and Xionggang Lu ^{1,2}

¹ State Key Laboratory of Advanced Special Steel, Shanghai 200072, China; nwx2006happy@163.com (W.N.); melo.lover@163.com (C.C.); wzhdng@shu.edu.cn (W.D.); luxg@shu.edu.cn (X.L.)

² Shanghai Key Laboratory of Advanced Ferrometallurgy, School of Materials Science and Engineering, Shanghai University, Shanghai 200072, China

* Correspondence: xjzou@shu.edu.cn (X.Z.); wxg228@shu.edu.cn (X.W.); Tel.: +86-21-5633-4005 (X.Z.); +86-21-5633-8244 (X.W.)

Academic Editors: Benoît Louis, Qiang Wang and Marcelo Maciel Pereira

Received: 6 March 2017; Accepted: 29 March 2017; Published: 31 March 2017

Abstract: Ni–Ce–Zr mixed oxides were prepared through one-pot hydrolysis of mixed metal nitrates with ammonium carbonate for CO₂ methanation. The effects of Ce/Zr molar ratio and Ni content on catalysts' physical and chemical properties, reduction degree of Ni²⁺, and catalytic properties were systematically investigated. The results showed that Zr could lower metallic Ni particle sizes and alter interaction between Ni and supports, resulting in enhancements in the catalytic activity for CO₂ methanation. The Ni–Ce–Zr catalyst containing 40 wt % Ni and Ce/Zr molar ratio of 9:1 exhibited the optimal catalytic properties, with 96.2% CO₂ conversion and almost 100% CH₄ selectivity at a low temperature of 275 °C. During the tested period of 500 h, CO₂ conversion and CH₄ selectivity over Ni–Ce–Zr catalyst kept constant under 300 °C.

Keywords: carbon dioxide; methanation; Ce–Zr oxide; nickel catalyst

1. Introduction

The increasing emissions of CO₂ have caused global warming and climate change, affecting human life and the ecological environment, due to the 'greenhouse effect'. Therefore, CO₂ fixation has attracted much interest in achieving a low carbon economy and society. Among the viable solutions to mitigate CO₂ emissions, many studies focused on two strategies: (i) CO₂ capture and sequestration; and (ii) CO₂ conversion to biofuels and high-value chemicals [1–3]. With regards to upcoming energy challenges, CO₂ conversion seems to be a more attractive and promising approach [2,3]. Considering that the consumption of fuels is two orders of magnitude higher than that of chemicals, CO₂ has to be mainly converted into energy carriers such as methane, methanol, and so on [4–9].

CO₂ methanation, also called the Sabatier reaction ($\text{CO}_2 + 4\text{H}_2 \leftrightarrow \text{CH}_4 + 2\text{H}_2\text{O}$, $\Delta H_{298\text{K}} = -164.7$ kJ/mol) [6], presents substantial advantages over CO₂ conversion to other fuels because methane can be injected directly into existing natural gas pipelines, or be used as a raw material for production of chemicals. For a reversible exothermic reaction, CO₂ methanation is required to perform at lower temperatures in order to obtain methane yield as high as possible. However, low temperature is favorable for CO disproportionation ($2\text{CO} \leftrightarrow \text{CO}_2 + \text{C}$, $\Delta H_{298\text{K}} = -172.4$ kJ/mol), resulting in coke deposition. Therefore, it is still a great challenge to develop a highly active and coke-resistant catalyst for CO₂ methanation.

Ni and noble metals like Ru, Pd and Rh, are reported to be the effective towards CO₂ methanation [10–24]. Ni-based catalysts are preferred as promising catalysts for this reaction due to

their high intrinsic activity and low cost [14–24]. However, supported Ni catalysts frequently suffer from severe deactivation due to particle sintering, interaction of metal particles with carbon monoxide, formation of mobile nickel subcarbonyls, and coke deposition [23]. Numerous investigations have been directed toward catalyst composition and support properties, which strongly influence the activity, stability and coke resistance of Ni catalysts [25,26].

In recent years, nickel-mixed oxides, especially Ni–Ce–Zr mixed oxides, have been believed to be among the potential catalysts for CO₂ methanation due to their high oxygen storage capacity and properties to activate CO₂ [21–24]. Nevertheless, these catalysts showed poor catalytic activity and stability under lower temperatures. It has been demonstrated that the catalytic properties of Ni-based catalysts can be improved by modifying catalyst supports, optimizing catalyst compositions, and improving catalyst preparation routes, etc. [25–28]. Ni–Ce–Zr mixed oxides were reported to prepare through citric sol–gel method [21,22], hydrothermal crystallization method [29] and co-precipitation method [30], etc. However, due to the addition of additional ligand, employing refluxed processing system and washing with distilled hot water, the preparation processes were complex and in high cost. Hence, there is still a great deal of interest in developing a simple one-step approach to fabrication of highly catalytic performance of Ni–Ce–Zr mixed oxides for CO₂ methanation.

In this paper, Ni–Ce–Zr mixed oxides were prepared through one-pot hydrolysis of mixed metal nitrates with ammonium carbonate. Effects of Ce/Zr molar ratio and Ni content on catalysts' physical and chemical properties, and reduction degree of Ni²⁺ were systematically investigated by XRD, N₂ adsorption, H₂-TPR. Their catalytic behavior for CO₂ methanation with H₂ in the range of 150–350 °C was intensively investigated to design an effective catalyst for CO₂ methanation.

2. Results and Discussion

2.1. Physicochemical Properties of Ni–Ce_{1-x}Zr_xO₂

The BET specific surface areas (*S*_{BET}) of the samples were summarized in Table 1. Compared with CeO₂, the addition of Ni and/or Zr to CeO₂ increased, which was consistent with literature reports [31]. The prepared *y*Ni–Ce_{1-x}Zr_xO₂ (except 40Ni–ZrO₂) samples by one-pot method, which contained redundant CeO₂, had specific surface areas of ca. 40–70 m² g⁻¹. The addition amounts of Ni and/or Zr did not change the *S*_{BET}, likely due to nickel or zirconium species does not significantly change the catalysts accessibility respect to CeO₂ [32].

Table 1. Physical properties of *y*Ni–Ce_{1-x}Zr_xO₂ catalysts and reaction results of CO₂ methanation.

| Catalysts | <i>S</i> _{BET} (m ² g ⁻¹) | Ni Crystallite Size (nm) ^a | X _{CO₂} (%) ^b | TOF (h ⁻¹) |
|---|---|---------------------------------------|--|------------------------|
| CeO ₂ | 27 | - | - | - |
| 40Ni–CeO ₂ | 64 | 27 | 4.2 | 0.08 |
| 40Ni–Ce _{0.95} Zr _{0.05} O ₂ | 53 | 21 | 7.1 | 0.18 |
| 40Ni–Ce _{0.9} Zr _{0.1} O ₂ | 46 | 18 | 10.3 | 0.31 |
| 40Ni–Ce _{0.8} Zr _{0.2} O ₂ | 68 | 18 | 10.5 | 0.30 |
| 40Ni–Ce _{0.7} Zr _{0.3} O ₂ | 56 | 19 | 10.8 | 0.28 |
| 40Ni–ZrO ₂ | 78 | 16 | 8.2 | 0.27 |
| Ce _{0.9} Zr _{0.1} O ₂ | 43 | - | - | - |
| 10Ni–Ce _{0.9} Zr _{0.1} O ₂ | 50 | 23 | 3.3 | 0.08 |
| 20Ni–Ce _{0.9} Zr _{0.1} O ₂ | 46 | 22 | 4.6 | 0.11 |
| 30Ni–Ce _{0.9} Zr _{0.1} O ₂ | 55 | 19 | 7.8 | 0.22 |
| 50Ni–Ce _{0.9} Zr _{0.1} O ₂ | 52 | 21 | 10.1 | 0.26 |

^a The catalysts were reduced at 800 °C for five and Ni crystallite size were estimated by XRD patterns; ^b Reaction conditions: GHSV, 28,000 mL g_{cat}⁻¹ h⁻¹; H₂/CO₂, 4; reaction temperature, 200 °C; reaction time one hour.

Figure 1 presents the XRD patterns of the 40Ni–Ce_{1-x}Zr_xO₂ (*x* = 0, 0.05, 0.1, 0.2, 0.3, 1) samples, together with those of CeO₂ and Ce_{0.9}Zr_{0.1}O₂ for comparison. CeO₂ sample showed a typical cubic

fluorite structure [21–23]. With the addition of Zr, the slight shifts to higher angles of four strong CeO₂ diffraction peaks around $2\theta = 28.6^\circ$, 33.1° , 47.5° and 56.4° and no reflections of ZrO₂ phase were observed in Ce_{0.9}Zr_{0.1}O₂ sample. The comparison of the XRD patterns for CeO₂ and Ce_{0.9}Zr_{0.1}O₂ revealed that Ce–Zr solid solution had been formed in the Ce_{0.9}Zr_{0.1}O₂ support [27,28]. Compared with CeO₂, NiO phase ($2\theta = 37.2^\circ$, 43.3° and 62.9° , corresponding to the (111), (200) and (220)) was observed and the diffraction peaks of CeO₂ had no shift of 40Ni–CeO₂ sample, implying that nickel was at least partially present as NiO species outside the fluorite structure. With the increasing of Zr, CeO₂ diffraction peaks shifted to higher angles of 40Ni–Ce_{1-x}Zr_xO₂ ($x = 0.05, 0.1, 0.2, 0.3, 1$) samples, attributing to Zr incorporating into the lattice of ceria to form a homogeneous Ce–Zr solid solution [27,28]. For low content of Zr, it was difficult to unequivocally identify formation of a solid solution, as a consequence of the expected slightly shifts to higher angles of CeO₂ diffraction peaks. And that, the introduction of higher amounts of Zr into the lattice reduced the observed d-spacing for the catalysts, and hence the diffraction peaks of CeO₂ shifted to higher angles distinctly. Furthermore, it was noted that the full width at half maximum (FWHM) of NiO (200) in 40Ni–Ce_{1-x}Zr_xO₂ ($x = 0.05, 0.1, 0.2, 0.3$) samples became wider than that of 40Ni–CeO₂, implying that Zr addition to 40Ni–CeO₂ decreased the NiO crystallites sizes.

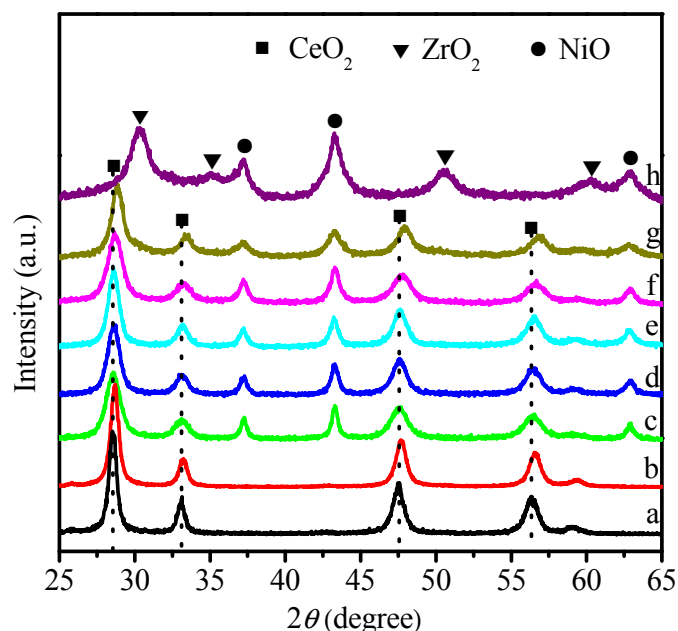


Figure 1. XRD patterns of the prepared samples calcined at 500 °C. (a) CeO₂; (b) Ce_{0.9}Zr_{0.1}O₂; 40Ni–Ce_{1-x}Zr_xO₂ with (c) $x = 0$; (d) $x = 0.05$; (e) $x = 0.1$; (f) $x = 0.2$; (g) $x = 0.3$ and (h) $x = 1$.

In order to analyze the effect of Ni content on the structure of y Ni–Ce_{1-x}Zr_xO₂ catalysts, the XRD patterns of y Ni–Ce_{0.9}Zr_{0.1}O₂ ($y = 10, 20, 30, 50$) catalysts were also analyzed and shown in Figure 2. All the samples showed similar XRD patterns to the corresponding Ce_{0.9}Zr_{0.1}O₂ supports except that the y Ni–Ce_{0.9}Zr_{0.1}O₂ ($y = 10, 20, 30, 40, 50$) catalysts exhibited NiO crystallites phase ($2\theta = 37.2^\circ$, 43.3° and 62.9°) with different relative intensity. The relative intensity of NiO diffraction peaks was enhanced with increasing Ni contents. No shifts of the diffraction peaks of CeO₂ were observed, meaning that the addition of Ni could not change the support structure, in accordance with the XRD results of 40Ni–Ce_{1-x}Zr_xO₂ samples. The result further confirmed that nickel was at least partially present as NiO species outside the fluorite structure.

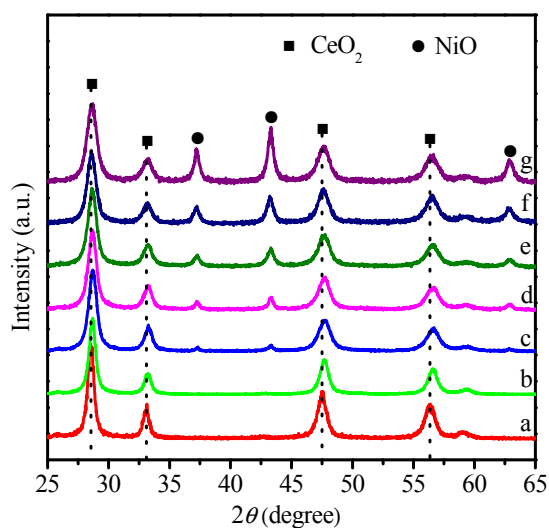


Figure 2. XRD patterns of the prepared samples calcined at 500 °C. (a) CeO_2 ; $y\text{Ni}-\text{Ce}_{0.9}\text{Zr}_{0.1}\text{O}_2$ with (b) $y = 0$; (c) $y = 10$; (d) $y = 20$; (e) $y = 30$; (f) $y = 40$; (g) $y = 50$.

TPR profiles of pure CeO_2 , and $40\text{Ni}-\text{Ce}_{1-x}\text{Zr}_x\text{O}_2$ ($x = 0, 0.05, 0.1, 0.2, 0.3$ and 1) samples calcined at 500 °C, were displayed in Figure 3. Pure CeO_2 and $40\text{Ni}-\text{Ce}_{1-x}\text{Zr}_x\text{O}_2$ ($x = 0, 0.05, 0.1, 0.2, 0.3$) samples showed a predominating reduction profile and a weak reduction peak, the maximum values of which were positioned in the temperature ranges of 300–500 °C and 760–950 °C, respectively. The former was ascribed to crystallized NiO on the support surface, and the latter is related to the reduction of CeO_2 supports. The single reduction band of NiO species represented a homogeneous metal–support interaction. Compared with $40\text{Ni}-\text{CeO}_2$ sample, the reduction peak temperatures for NiO species in TPR profiles increased with increasing Zr contents, implying that Zr addition resulted in strengthening of metal–support interaction. In terms of the $40\text{Ni}-\text{ZrO}_2$ sample, the H_2 -TPR profile showed two reductive peaks centered at ca. 405 °C and 603 °C, respectively. The former was ascribed to the reduction of free NiO particles and the latter was related to the reduction of crystallized NiO which had a strong interaction with the ZrO_2 support, implying heterogeneous metal–support interaction. From these observations in combination with XRD patterns in Figure 1, we could reasonably infer that the addition of Zr to Ni– CeO_2 could form Ce–Zr solid solution and meanwhile alter the interaction between Ni and $\text{Ce}_{1-x}\text{Zr}_x\text{O}_2$ support.

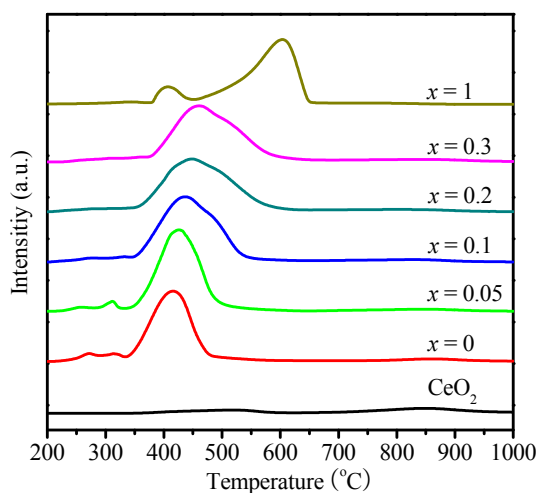


Figure 3. H_2 -TPR profiles of CeO_2 and $40\text{Ni}-\text{Ce}_{1-x}\text{Zr}_x\text{O}_2$ samples.

The TPR profiles of $y\text{Ni}-\text{Ce}_{0.9}\text{Zr}_{0.1}\text{O}_2$ ($y = 10, 20, 30, 50$) catalysts were also shown in Figure 4. All the $y\text{Ni}-\text{Ce}_{0.9}\text{Zr}_{0.1}\text{O}_2$ samples showed a H_2 consumption peak positioned in the temperature range of 350–550 °C, corresponding to the reduction of crystallized NiO which had an interaction with the $\text{Ce}_{0.9}\text{Zr}_{0.1}\text{O}_2$ support. The H_2 consumption peak of NiO had no discernible shift and the peak intensity increase in Ni content. The hydrogen consumptions obtained by the integration of the peak areas increased in proportion to Ni content. These results implied the metal-support interaction had no change with increasing Ni content in accordance with the XRD results in Figure 1. NiO could be almost reduced to metallic Ni under the reduction conditions.

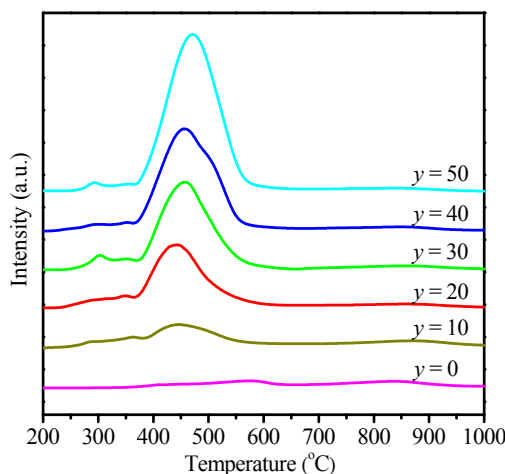


Figure 4. H_2 -TPR profiles of the $y\text{Ni}-\text{Ce}_{0.9}\text{Zr}_{0.1}\text{O}_2$ samples.

It was well known that metallic Ni atoms were active sites for CO_2 methanation and Ni-based catalysts should be pre-reduced to form metallic Ni before the methanation reaction. Ni crystallite sizes had close relationships with the activity, the stability, and the resistance to carbon deposition of the catalysts for CO_2 methanation. The preliminary results showed that $40\text{Ni}-\text{Ce}_{1-x}\text{Zr}_x\text{O}_2$ catalysts reduced at 500 °C for two hours had the optimum catalytic performance for CO_2 reforming. Herein the XRD patterns of the $40\text{Ni}-\text{Ce}_{1-x}\text{Zr}_x\text{O}_2$ ($x = 0, 0.05, 0.1, 0.2, 0.3, 1$) catalysts, together with those of CeO_2 and $\text{Ce}_{0.9}\text{Zr}_{0.1}\text{O}_2$ samples reduced at 500 °C in a H_2 flow were displayed in Figure 5. It could be seen that the XRD patterns of the CeO_2 and $\text{Ce}_{0.9}\text{Zr}_{0.1}\text{O}_2$ samples reduced were almost the same as the corresponding calcined samples. In case of $40\text{Ni}-\text{Ce}_{1-x}\text{Zr}_x\text{O}_2$, there were three new diffraction peaks at 44.5° , 51.8° and 76.4° corresponding to Ni (111), (200) and (220) reflections, respectively. Correspondingly, the peaks of NiO phase disappeared, indicating that NiO were nearly reduced to metallic Ni, as the TPR results. The Ni diffraction peaks width increased with the addition of Zr, implying that the reduction of the Ni crystallite sizes decreased. As a result, the apparent Ni crystallite sizes estimated from broadening of the Ni (1 1 1) reflection using the Scherrer formula were listed in Table 1. The $40\text{Ni}-\text{CeO}_2$ catalyst had an average Ni crystallite size of 27 nm, larger than that of 20 nm for $40\text{Ni}-\text{Ce}_{0.95}\text{Zr}_{0.05}\text{O}_2$, and then the Ni crystallite sizes slightly decreased from 20 to 18 nm with raising Zr molar fraction from 0.05 to 0.1 in the $40\text{Ni}-\text{Ce}_{1-x}\text{Zr}_x\text{O}_2$ catalysts. With the further increasing Zr content, Ni crystallite sizes slightly increased. These results indicated that addition of Zr could improve the dispersion of Ni species on the catalyst surface as reported in the literatures [27]. $y\text{Ni}-\text{Ce}_{0.9}\text{Zr}_{0.1}\text{O}_2$ ($y = 10, 20, 30, 50$) catalysts with different Ni content were reduced under the present conditions and the XRD patterns were shown in Figure 6. Ni crystallite sizes of $y\text{Ni}-\text{Ce}_{0.9}\text{Zr}_{0.1}\text{O}_2$ ($y = 10, 20, 30, 50$) catalysts estimated using the Scherrer formula were also displayed in Table 1. Ni crystallite sizes decreased from 23 to 18 nm when the Ni content was raised from 10 to 40%, and then Ni crystallite sizes increased to 21 nm with further increasing Ni content to 50%. These results indicate that if the nickel content was excessively high, a portion of the Ni particles agglomerate

instead of interacting with the support. As a whole, Ni crystallite sizes had no obvious aggregation and growth with the increasing Ni content, indicating that the preparation method was suitable for preparing high-loaded Ni-based catalysts with acceptable Ni crystallite sizes.

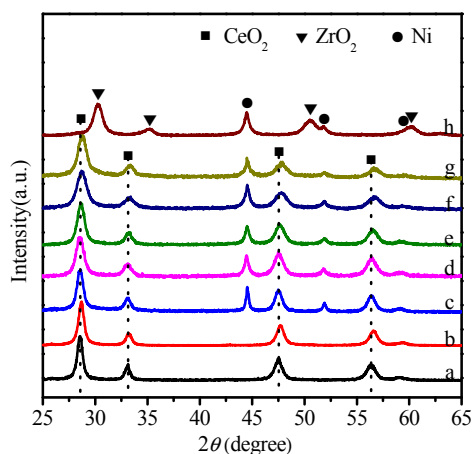


Figure 5. XRD patterns of the prepared samples reduced at 500 °C. (a) CeO₂; (b) Ce_{0.9}Zr_{0.1}O₂; 40Ni–Ce_{1–x}Zr_xO₂ with (c) $x = 0$; (d) $x = 0.05$; (e) $x = 0.1$; (f) $x = 0.2$; (g) $x = 0.3$ and (h) $x = 1$.

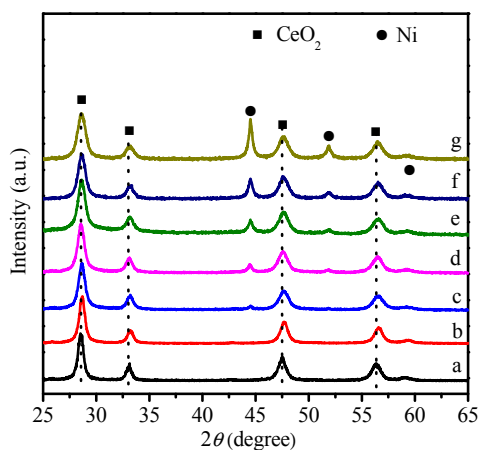


Figure 6. XRD patterns of the prepared samples reduced at 500 °C. (a) CeO₂; y Ni–Ce_{0.9}Zr_{0.1}O₂ with (b) $y = 0$; (c) $y = 10$; (d) $y = 20$; (e) $y = 30$; (f) $y = 40$; (g) $y = 50$.

2.2. Catalysis Reaction

The catalytic performance of the prepared catalysts was investigated for CO₂ methanation. For all tested catalyst, the CH₄ selectivities were found to be >99.9%. Therefore, only CO₂ conversions were shown to evaluate the catalytic performance.

In order to study the effect of the preparation method, 40Ni–Ce_{0.9}Zr_{0.1}O₂, 40Ni–Ce_{0.9}Zr_{0.1}O₂-SC, 40Ni–Ce_{0.9}Zr_{0.1}O₂-SH, 40Ni–Ce_{0.9}Zr_{0.1}O₂-AH, and 40Ni–Ce_{0.9}Zr_{0.1}O₂-imp were firstly investigated for CO₂ methanation with a H₂ to CO₂ molar ratio of four and GHSV of 3000 mL g_{cat}^{−1} h^{−1} under 150–350 °C. Figure 7 presented CO₂ conversion versus temperature. 40Ni–Ce_{0.9}Zr_{0.1}O₂ prepared through one-pot hydrolysis of mixed metal nitrates with ammonium carbonate exhibited the highest catalytic activity in comparison to other preparation methods in all tested reaction temperature range. Moreover, it was found that the maximal levels of CO₂ conversion in the presence of the 40Ni–Ce_{0.9}Zr_{0.1}O₂ catalyst was 97.0% at 275 °C, which reached chemical equilibrium value. In the case of the 40Ni–Ce_{0.9}Zr_{0.1}O₂-SC, 40Ni–Ce_{0.9}Zr_{0.1}O₂-SH, 40Ni–Ce_{0.9}Zr_{0.1}O₂-AH,

and $40\text{Ni-Ce}_{0.9}\text{Zr}_{0.1}\text{O}_2\text{-imp}$ catalysts, however, the highest CO_2 conversion (ca. 92.0%) were obtained under $350\text{ }^\circ\text{C}$.

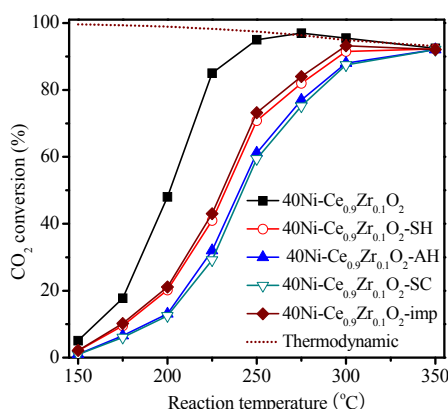


Figure 7. Catalytic performance of the $40\text{Ni-Ce}_{0.9}\text{Zr}_{0.1}\text{O}_2$ catalysts prepared by different methods for CO_2 methanation. Reaction conditions: GHSV, $3000\text{ mL g}_{\text{cat}}^{-1}\text{ h}^{-1}$; H_2/CO_2 , 4.

The $y\text{Ni-Ce}_{1-x}\text{Zr}_x\text{O}_2$ catalysts prepared through one-pot hydrolysis of mixed metal nitrates with ammonium carbonate were investigated in detail. The effect of catalyst composition on the performance of CO_2 methanation was investigated and the results were presented in Figure 8. CO_2 conversion rapidly increased with elevating the reaction temperature and reached the highest value at $275\text{ }^\circ\text{C}$ on all tested catalysts. However, if the reaction temperature was further increased to $350\text{ }^\circ\text{C}$, the catalytic activity started to decline. It was generally known that the CO_2 conversion would decrease at unnecessarily high temperatures because of the endothermic and reverse reaction. In Figure 8a, it could be seen that 40Ni-CeO_2 showed 88.0% CO_2 conversion at $250\text{ }^\circ\text{C}$. With raising Zr molar fraction to 0.1, CO_2 conversion increased to 95.0%, very close to chemical equilibrium value ($\sim 97.5\%$). As the Zr molar fraction was further increased to 0.3, the catalytic activity was almost kept unchanged. The enhancement of catalytic activity with Zr content was likely responsible for smaller metallic Ni particle sizes and the interaction of Ni with supports on $40\text{Ni-Ce}_{1-x}\text{Zr}_x\text{O}_2$ ($x = 0.05, 0.1, 0.2, 0.3$) catalysts. The effect of Ni content on catalytic performance of the $y\text{Ni-Ce}_{0.9}\text{Zr}_{0.1}\text{O}_2$ catalysts for CO_2 methanation was shown in Figure 8b. CO_2 conversion increased with increasing Ni content from 10 to 40%. Further increasing Ni content to 50%, CO_2 conversion slightly decreased. These results were well consistent with the crystallite sizes of metallic Ni.

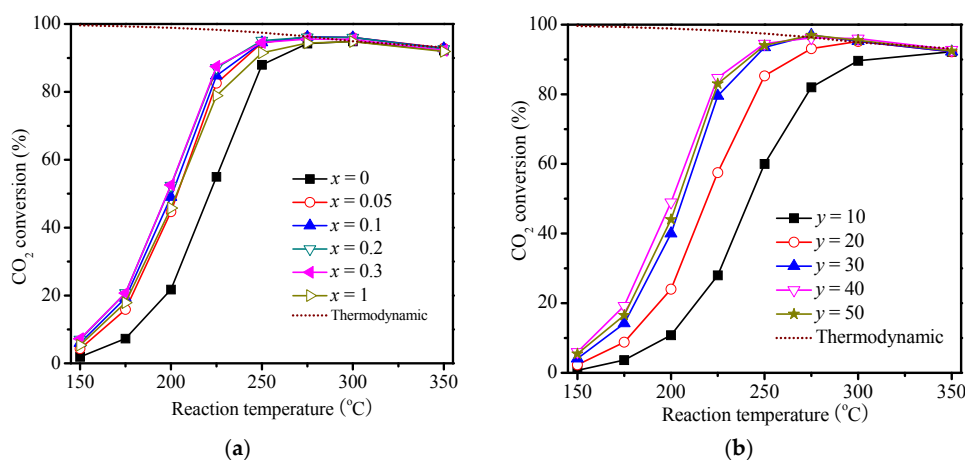


Figure 8. Catalytic performance of (a) $40\text{Ni-Ce}_{0.9}\text{Zr}_{0.1}\text{O}_2$ and (b) $y\text{Ni-Ce}_{0.9}\text{Zr}_{0.1}\text{O}_2$ catalysts for CO_2 methanation. Reaction conditions: GHSV, $3000\text{ mL g}_{\text{cat}}^{-1}\text{ h}^{-1}$; H_2/CO_2 , 4.

In order to further analyze the interrelation between the catalytic properties and Ni active sites over $y\text{Ni}-\text{Ce}_{1-x}\text{Zr}_x\text{O}_2$ for CO_2 methanation, turnover frequencies (TOFs), which reflect the intrinsic activity of the active sites in the catalyst, were carried out at a high GHSV to obtain a low CO_2 conversion ($\leq 10\%$), where the possibility of either the external or internal diffusion limitations were almost completely eliminated. Table 1 summarized the corresponding TOFs over the $y\text{Ni}-\text{Ce}_{1-x}\text{Zr}_x\text{O}_2$ catalysts for the CO_2 methanation. For $40\text{Ni}-\text{Ce}_{1-x}\text{Zr}_x\text{O}_2$ ($x = 0.05, 0.1, 0.2, 0.3$) catalysts, it could be seen that the TOF was higher than that of $40\text{Ni}-\text{CeO}_2$ catalyst. It could be seen that the TOFs gradually increased from 0.18 h^{-1} to 0.31 h^{-1} with the increase in the Zr molar fraction from 0.05 to 0.1. With further increasing Zr molar fraction to 0.3, the TOFs slightly decreased from 0.31 h^{-1} to 0.28 h^{-1} . The TOFs showed a reverse trend from the Ni crystallite size. However, in the case of $40\text{Ni}-\text{ZrO}_2$ showing smaller Ni crystallite size than $40\text{Ni}-\text{Ce}_{0.9}\text{Zr}_{0.1}\text{O}_2$ catalysts, the TOF was found lower than that of $40\text{Ni}-\text{Ce}_{0.9}\text{Zr}_{0.1}\text{O}_2$. Combined with the TPR result, it could be speculated that the intrinsic rates for the CO_2 methanation over the $40\text{Ni}-\text{Ce}_{1-x}\text{Zr}_x\text{O}_2$ not only depended on the Ni crystallite sizes, but also had a strong correlation with interaction of Ni with supports. Moreover, for $y\text{Ni}-\text{Ce}_{0.9}\text{Zr}_{0.1}\text{O}_2$ catalysts, Ni contents could not alter the interaction of Ni and $\text{Ce}_{0.9}\text{Zr}_{0.1}\text{O}_2$ support and the TOFs matched well with the metallic Ni particle sizes. It was speculated that Zr could improve lower metallic Ni particle sizes and alter the interaction between Ni and supports, resulting in enhancements in the activity and stability for CO_2 methanation.

The stability tests were carried out for the CO_2 methanation at $300 \text{ }^\circ\text{C}$ and $\text{GHSV} = 28,000 \text{ mL g}_{\text{cat}}^{-1} \text{ h}^{-1}$ with a H_2 to CO_2 molar ratio of four over $40\text{Ni}-\text{Ce}_{0.9}\text{Zr}_{0.1}\text{O}_2$ catalyst. Figure 9 showed the catalytic performance as a function of reaction time. It could be seen that $40\text{Ni}-\text{Ce}_{0.9}\text{Zr}_{0.1}\text{O}_2$ catalyst exhibited good stability under the operating conditions. During the tested period of 500 h, the CO_2 conversion and CH_4 selectivity were constant at ca. 87% and 100% respectively. To the best of our knowledge, this was the first example of Ni-based catalyst, which showed not only high activity but also superior long-term stability at $300 \text{ }^\circ\text{C}$.

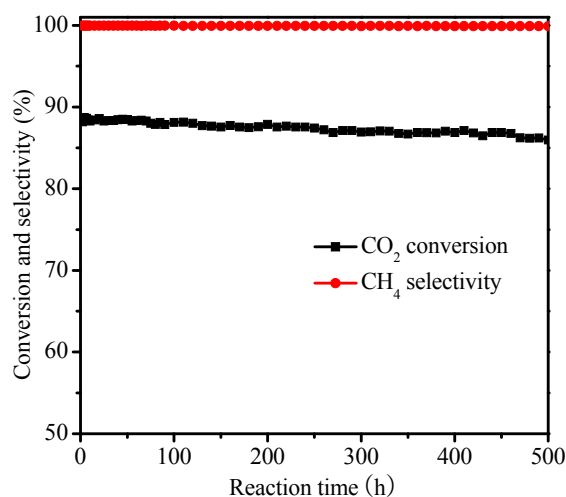


Figure 9. Stability of the prepared $40\text{Ni}-\text{Ce}_{0.9}\text{Zr}_{0.1}\text{O}_2$ catalysts for CO_2 methanation. Reaction conditions: $\text{GHSV}, 28,000 \text{ mL g}_{\text{cat}}^{-1} \text{ h}^{-1}$; $\text{H}_2/\text{CO}_2, 4$; reaction temperature, $300 \text{ }^\circ\text{C}$.

It has been established that carbon deposition is mainly responsible for the deactivation of Ni-based catalysts. Thus, the amount of carbon deposition on the used catalyst was investigated by TG (not shown). Only trace amounts of carbon were deposited on the catalyst. The percentage of the deposited carbon was less than $0.01 \text{ mg g}_{\text{cat}}^{-1} \text{ h}^{-1}$. XRD analysis was carried out over the $40\text{Ni}-\text{Ce}_{0.9}\text{Zr}_{0.1}\text{O}_2$ catalyst for CO_2 methanation at $300 \text{ }^\circ\text{C}$ after a reaction time of 500 h (not shown). Compared with before the reaction, the XRD patterns of the used $40\text{Ni}-\text{Ce}_{0.9}\text{Zr}_{0.1}\text{O}_2$ almost remained unchanged and no growth of Ni particle sizes was observed, which was also confirmed by TEM result

shown in Figure 10. These results demonstrated that the 40Ni–Ce_{0.9}Zr_{0.1}O₂ catalyst possessed a stable structure and the Ni particle sizes were retained during the reaction process.

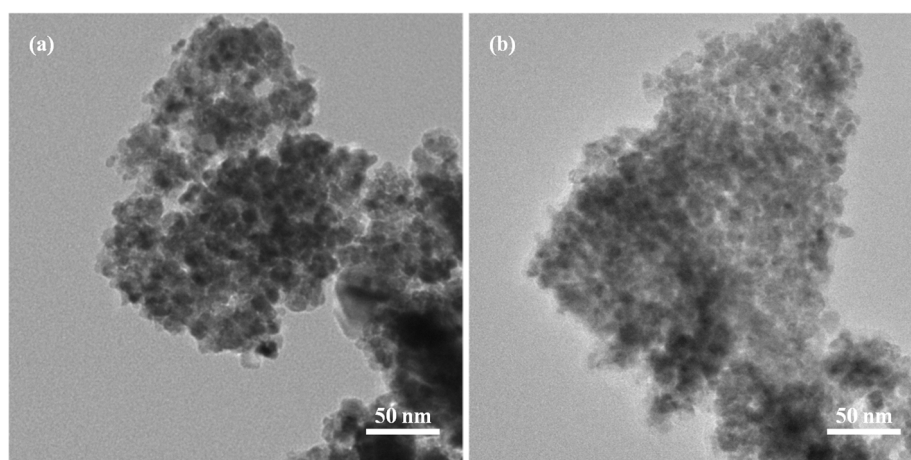


Figure 10. TEM image of the 40Ni–Ce_{0.9}Zr_{0.1}O₂ catalyst. (a) Reduced at 600 °C for two hours; (b) after 500 h reaction at 300 °C.

3. Materials and Methods

3.1. Material Preparation

Ni–Ce–Zr mixed oxides were prepared via one-pot hydrolysis of mixed metal nitrates with ammonium carbonate ((NH₄)₂CO₃). In a typical synthesis, 50 mL of a mixed aqueous solution of metal nitrates with a total metal [Ce + Zr] ion concentration of 0.2 mol L⁻¹ and a required Ni ion concentration was heated to 80 °C. 100 mL of 2 mol L⁻¹ (NH₄)₂CO₃ aqueous solution was directly poured into the mixed aqueous solution of metal nitrates with vigorous magnetic stirring, and at this time, the pH value of the mixture was measured at 8.8–9.0. The mixture was continuously stirred at 80 °C until the water was evaporated out. The obtained solid was dried at 100 °C overnight, and calcined at 500 °C for 5 h in air. The prepared catalysts were denoted as *y*Ni–Ce_{1–*x*}Zr_{*x*}O₂, where *x* represented Zr molar fraction of the total molar of Ce and Zr, and *y* represented the content of Ni in wt %.

In order to carry out a comparison study, 40% Ni supported on Ce_{0.9}Zr_{0.1}O₂ were synthesized via one-pot hydrolysis of mixed metal nitrates with three other hydrolysis agents (sodium carbonate, sodium hydroxide and ammonium hydroxide). In detail, 50 mL of a mixed aqueous solution with 0.009 mol Ce(NO₃)₃·6H₂O, 0.001 mol Zr(NO₃)₄·5H₂O and 0.0189 mol Ni(NO₃)₂·6H₂O was heated to 80 °C. 2 mol L⁻¹ hydrolysis agent (sodium carbonate, sodium hydroxide, ammonium hydroxide) aqueous solution was respectively dropped into the aqueous solution of inorganic salts with vigorous magnetic stirring until the pH value of the mixture was measured in the range of 8.8–9.0. The resulted precipitate, prepared with sodium carbonate and sodium hydroxide, was filtered and washed with distilled water, then dried at 100 °C overnight, and finally calcined at 500 °C for 5 h in air, which was denoted as 40Ni–Ce_{0.9}Zr_{0.1}O₂-SC and 40Ni–Ce_{0.9}Zr_{0.1}O₂-SH respectively. The resulted precipitate prepared with ammonium hydroxide was continuously stirred at 80 °C until the water was evaporated out. The obtained solid was dried at 100 °C overnight, and finally calcined at 500 °C for 5 h in air. The prepared catalysts were denoted as 40Ni–Ce_{0.9}Zr_{0.1}O₂-AH.

The other sample containing 40 wt % Ni, denoted 40Ni–Ce_{0.9}Zr_{0.1}O₂-imp catalyst was prepared by an incipient impregnation method. Ce_{0.9}Zr_{0.1}O₂ powder prepared via one-pot hydrolysis of mixed metal nitrates with (NH₄)₂CO₃ was added into an aqueous solution of Ni(NO₃)₂ under stirring and kept at ambient temperature for 2 h. The mixture was evaporated out 80 °C and then dried at 100 °C overnight, and finally calcined at 500 °C for 5 h in air.

3.2. Material Characterization

BET surface areas of the catalysts were measured by N₂ adsorption–desorption using a Micromeritics ASAP 2020 Sorptometer (Micromeritics Instrument Corp., Norcross, GA, USA) at liquid nitrogen temperature (−196 °C). Before the measurement, each sample was degassed to eliminate volatile adsorbents on the surface at 300 °C for 6 h.

Powder X-ray diffraction (XRD) was performed with a D/Max-2550 diffractometer (Rigaku, Tokyo, Japan) using Cu K α radiation (40 kV, 200 mA). The crystallite sizes of metallic Ni were estimated using the full-widths at half maximum (FWHM) of the Ni (111) peak through the Scherrer equation, as reported in our previous work [33,34].

Temperature-programmed reduction with H₂ (H₂-TPR) was performed on a homemade equipment to observe the reducibility of the catalysts. TPR measurements were carried out with 0.1 g of catalyst, placed in a quartz reactor and first pretreated in an Ar stream (30 mL min^{−1}) at 300 °C for 0.5 h to remove moisture and other absorbed impurities, and then cooled to 200 °C. The temperature was raised to 1000 °C at a heating rate of 10 °C min^{−1}. The amount of H₂ uptake was measured with a thermal conductivity detector (TCD) (Shanghai Kechuang Chromatograph Instruments Co., Ltd., Shanghai, China).

The amount of carbon deposition on the used samples was determined with a thermogravimetric analyzer (TG) (Netzsch STA 4449 F3) (Netzsch Scientific Instruments Trading, Sedanstraße, Germany). The used catalysts were pre-treated at 50 °C for 30 min and then heated up to 800 °C with a rate of 10 °C min^{−1} in an air flow of 30 mL min^{−1}.

Transmission electron microscope (TEM) micrographs were obtained with a JEM-2010F (JEOL Ltd., Kyoto, Japan) field emission microscope operating at 200 kV. The sample was prepared by placing a drop of the ethanol solution of a well-ground catalyst powder on a carbon-coated copper grid (300 mesh), followed by evaporation of the ethanol.

3.3. Catalytic Test

CO₂ methanation was performed in a vertical continuous-flow fixed-bed reactor (inner diameter of 8 mm and a length of 800 mm) at atmospheric pressure. The reaction gases were controlled using mass flow controllers. The actual temperature of the catalyst was monitored using a thermocouple placed in the middle of the catalyst bed. Two hundred milligrams of catalyst diluted with 800 mg of quartz particles (60–80 mesh) was placed between two layers of quartz wool in the center of the reactor. Prior to the reaction, the catalyst was first reduced in situ at 500 °C at a heating rate of 10 °C min^{−1} under a 20 mL min^{−1} flow of H₂ for 2 h and then cooled to the set reaction temperature (150–350 °C). The effluent gas was cooled in a condenser at room temperature and passed a diorite bed to remove all water. Finally, the dried gas products were analyzed using an on-line GC-TCD chromatograph using TDX-01 and Molecular Sieve 5A packed column (Shanghai Kechuang Chromatograph Instruments Co., Ltd., Shanghai, China). The flow rate of the outlet gas was measured by a soap flow meter. The overall mass balance was more than 98% on the basis of carbon in the starting reactants.

On the basis of the carbon balance in the effluent gas under assumption of no carbon deposition, the conversion of CO₂ was defined as the percentage of the total molar flow rate of CH₄ and CO in the exit gas to the molar flow rate of CO₂ in the feed gas. The selectivity of the CH₄ (or CO) was designated as the percentage of the molar of CH₄ (or CO) in the total molar of the CH₄ and CO.

The turnover frequencies (TOFs) of the $y\text{Ni}-\text{Ce}_{1-x}\text{Zr}_x\text{O}_2$ catalysts for the CO₂ methanation are defined as the number of converted CO₂ molecules per metal Ni atom and hour. In order to precisely determine the intrinsic reaction rate on the metal active sites, the TOFs of the $y\text{Ni}-\text{Ce}_{1-x}\text{Zr}_x\text{O}_2$ catalysts were carried out at a high gas hourly space velocity (GHSV) to obtain a low CO₂ conversion ($\leq 10\%$). For this, a 50 mg catalyst powder diluted with 200 mg of quartz powder was used for the reaction with GHSV of 28,000 mL g_{cat}^{−1} h^{−1} under 200 °C.

On the assumption that all Ni ions were completely reduced into metallic Ni atoms and formed spherical particles with a diameter (d_{XRD}) determined by the Scherrer equation to the Ni (111)

diffraction peaks, and the distance between metal atoms in Ni crystallites was assumed to be 0.249 nm. TOF was calculated by the equation as follows:

$$\text{TOF} = \left(\frac{N_{\text{CO}_2, \text{in}}}{N_{\text{Ni}}} \times X_{\text{CO}_2} \right) \times \left(\frac{d_{\text{XRD}}^3}{d_{\text{XRD}}^3 - (d_{\text{XRD}} - 0.498)^3} \right) \text{h}^{-1}$$

where N_{CO_2} : the flow rate of CO_2 in mol h^{-1} in the feed; N_{Ni} : the mole number of Ni in 50 mg catalyst.

4. Conclusions

$y\text{Ni}-\text{Ce}_{1-x}\text{Zr}_x\text{O}_2$ catalysts were successfully prepared through the one-pot hydrolysis of mixed metal nitrates with $(\text{NH}_4)_2\text{CO}_3$ method. The catalysts showed excellent low-temperature activity and stability in CO_2 methanation in the temperature range of 150–350 °C. The catalytic performance not only depended on the Ni crystallite sizes, but also had a strong correlation with interaction of Ni with supports. Zr addition to Ni– CeO_2 affected reducibility of Ni^{2+} ions, the Ni crystallite sizes formed, and interaction between Ni and supports, resulting in excellent catalytic activity, stability and anti-coking ability. The 40Ni– $\text{Ce}_{0.9}\text{Zr}_{0.1}\text{O}_2$ catalyst exhibited optimal catalytic properties. The stability test showed that 40Ni– $\text{Ce}_{0.9}\text{Zr}_{0.1}\text{O}_2$ retained long-term stability without deterioration during the 500 h reaction period. These results will be helpful to develop highly effective Ni-based catalysts for low temperature CO_2 methanation.

Acknowledgments: This research was supported by Innovation Program of Shanghai Municipal Education Commission, the Major State Basic Research Development Program of China (No. 2014CB643403), National Science Fund for Distinguished Young Scholars (No. 51225401) and Basic Major Research Program of Science and Technology Commission Foundation of Shanghai (No. 14JC1491400).

Author Contributions: Xueguang Wang and Xiujing Zou conceived and designed the experiments; Wangxin Nie performed the experiments; Xueguang Wang, Xiujing Zou, Weizhong Ding and Xionggang Lu interpreted and analyzed the data; Wangxin Nie and Chenju Chen contributed reagents/materials/analysis tools; Xiujing Zou wrote the manuscript.

Conflicts of Interest: The authors declare no conflict of interest.

References

1. Ferey, G.; Serr, C.; Devic, T.; Maurin, G.; Jolic, H.; Llewellyn, P.L.; De Weireld, G.; Vimont, A.; Daturi, M.; Chang, J.S. Why hybrid porous solids capture greenhouse gases? *Chem. Soc. Rev.* **2011**, *40*, 550–562. [[CrossRef](#)] [[PubMed](#)]
2. Hunt, A.J.; Sin, E.H.K.; Marriott, R.; Clark, J.H. Generation, capture, and utilization of industrial carbon dioxide. *ChemSusChem* **2010**, *3*, 306–322. [[CrossRef](#)] [[PubMed](#)]
3. Mikkelsen, M.; Jorgensen, M.; Krebs, F.C. The teraton challenge. A review of fixation and transformation of carbon dioxide. *Energy Environ. Sci.* **2010**, *3*, 43–81. [[CrossRef](#)]
4. Porosoff, M.D.; Yan, B.H.; Chen, J.G. Catalytic reduction of CO_2 by H_2 for synthesis of CO, methanol and hydrocarbons: Challenges and opportunities. *Energy Environ. Sci.* **2016**, *9*, 62–73. [[CrossRef](#)]
5. Wang, W.; Wang, S.P.; Ma, X.B.; Gong, J.L. Recent advances in catalytic hydrogenation of carbon dioxide. *Chem. Soc. Rev.* **2011**, *40*, 3703–3727. [[CrossRef](#)] [[PubMed](#)]
6. Gao, J.J.; Liu, Q.; Gu, F.N.; Liu, B.; Zhong, Z.Y.; Su, F.B. Recent advances in methanation catalysts for the production of synthetic natural gas. *RSC Adv.* **2015**, *5*, 22759–22776. [[CrossRef](#)]
7. Aziz, M.A.A.; Jalil, A.A.; Triwahyono, S.; Ahmad, A. CO_2 methanation over heterogeneous catalysts: Recent progress and future prospects. *Green Chem.* **2015**, *17*, 2647–2663. [[CrossRef](#)]
8. Frontera, P.; Macario, A.; Ferraro, M.; Antonucci, P. Supported catalysts for CO_2 methanation: A review. *Catalysts* **2017**, *7*, 59. [[CrossRef](#)]
9. Fechet, I.; Vedrine, J.C. Nanoporous materials as new engineered catalysts for the synthesis of green fuels. *Molecules* **2015**, *20*, 5638–5666. [[CrossRef](#)] [[PubMed](#)]
10. Abe, T.; Tanizawa, M.; Watanabe, K.; Taguchi, A. CO_2 methanation property of Ru nanoparticle-loaded TiO_2 prepared by a polygonal barrel-sputtering method. *Energy Environ. Sci.* **2009**, *2*, 315–321. [[CrossRef](#)]

11. Karelavic, A.; Ruiz, P. CO₂ hydrogenation at low temperature over Rh/ γ -Al₂O₃ catalysts: Effect of the metal particle size on catalytic performances and reaction mechanism. *Appl. Catal. B* **2012**, *113–114*, 237–249. [[CrossRef](#)]
12. Jacquemin, M.; Beuls, A.; Ruiz, P. Catalytic production of methane from CO₂ and H₂ at low temperature: Insight on the reaction mechanism. *Catal. Today* **2010**, *157*, 462–466. [[CrossRef](#)]
13. Zhu, Y.; Zhang, S.; Ye, Y.; Zhang, X.; Wang, L.; Zhu, W.; Cheng, F.; Tao, F. Catalytic conversion of carbon dioxide to methane on ruthenium–cobalt bimetallic nanocatalysts and correlation between surface chemistry of catalysts under reaction conditions and catalytic performances. *ACS Catal.* **2012**, *2*, 2403–2408. [[CrossRef](#)]
14. Yan, Y.; Dai, Y.H.; He, H.; Yu, Y.B.; Yang, Y.H. A novel W-doped Ni-Mg mixed oxide catalyst for CO₂ methanation. *Appl. Catal. B Environ.* **2016**, *196*, 108–116. [[CrossRef](#)]
15. Wierzbicki, D.; Debek, R.; Motak, M.; Grzybek, T.; Gálvez, M.E.; Da Costa, P. Novel Ni-La-hydrotralcite derived catalysts for CO₂ methanation. *Catal. Commun.* **2016**, *83*, 5–8. [[CrossRef](#)]
16. Xu, L.L.; Wang, F.G.; Chen, M.D.; Zhang, J.K.; Yuan, D.; Wang, L.J.; Wu, K.; Xu, G.Q.; Chen, W. CO₂ methanation over a Ni based ordered mesoporous catalyst for the production of synthetic natural gas. *RSC Adv.* **2016**, *6*, 28489–28499. [[CrossRef](#)]
17. Du, G.A.; Lim, S.; Yang, Y.H.; Wang, C.; Pfefferle, L.; Haller, G.L. Methanation of carbon dioxide on Ni-incorporated MCM-41 catalysts: The influence of catalyst pretreatment and study of steady-state reaction. *J. Catal.* **2007**, *249*, 370–379. [[CrossRef](#)]
18. Zhi, G.J.; Guo, X.N.; Wang, Y.Y.; Jin, G.Q.; Guo, X.Y. Effect of La₂O₃ modification on the catalytic performance of Ni/SiC for methanation of carbon dioxide. *Catal. Commun.* **2011**, *16*, 56–59. [[CrossRef](#)]
19. Graca, I.; Gonzalez, L.V.; Bacariza, M.C.; Fernandes, A.; Henriques, C.; Lopes, J.M.; Ribeiro, M.F. CO₂ hydrogenation into CH₄ on NiHNaUSY zeolites. *Appl. Catal. B Environ.* **2014**, *147*, 101–110. [[CrossRef](#)]
20. Abello, S.; Berrueco, C.; Montane, D. High-loaded nickel-alumina catalyst for direct CO₂ hydrogenation into synthetic natural gas (SNG). *Fuel* **2013**, *113*, 598–609. [[CrossRef](#)]
21. Ocampo, F.; Louis, B.; Kiwi-Minsker, L.; Roger, A.C. Effect of Ce/Zr composition and noble metal promotion on nickel based Ce_xZr_{1-x}O₂ catalysts for carbon dioxide methanation. *Appl. Catal. A Gen.* **2011**, *392*, 36–44. [[CrossRef](#)]
22. Ocampo, F.; Louis, B.; Roger, A.C. Methanation of carbon dioxide over nickel-based Ce_{0.72}Zr_{0.28}O₂ mixed oxide catalysts prepared by sol-gel method. *Appl. Catal. A Gen.* **2009**, *369*, 90–99. [[CrossRef](#)]
23. Cai, W.; Zhong, Q.; Zhao, Y.X. Fractional-hydrolysis-driven formation of non-uniform dopant concentration catalyst nanoparticles of Ni/Ce_xZr_{1-x}O₂ and its catalysis in methanation of CO₂. *Catal. Commun.* **2013**, *39*, 30–34. [[CrossRef](#)]
24. Pan, Q.; Peng, J.; Sun, T.; Gao, D.; Wang, S.; Wang, S. CO₂ methanation on Ni/Ce_{0.5}Zr_{0.5}O₂ catalysts for the production of synthetic natural gas. *Fuel Process. Technol.* **2014**, *123*, 166–171. [[CrossRef](#)]
25. Muroyama, H.; Tsuda, Y.; Asakoshi, T.; Masitah, H.; Okanishi, T.; Matsui, T.; Eguchi, K. Carbon dioxide methanation over Ni catalysts supported on various metal oxides. *J. Catal.* **2016**, *343*, 178–184. [[CrossRef](#)]
26. Du, Y.L.; Wu, X.; Cheng, Q.; Huang, Y.L.; Huang, W. Development of Ni-based catalysts derived from hydrotralcite-like compounds precursors for synthesis gas production via methane or ethanol reforming. *Catalysts* **2017**, *7*, 70. [[CrossRef](#)]
27. Zhang, Y.; Wang, R.; Lin, X.; Wang, Z.; Liu, J.; Zhou, J.; Cen, K. Effects of Ce/Zr composition on nickel based Ce_(1-x)Zr_xO₂ catalysts for hydrogen production in sulfur-iodine cycle. *Int. J. Hydrog. Energy* **2014**, *39*, 10853–10860. [[CrossRef](#)]
28. Kramer, M.; Stowe, K.; Duisberg, M.; Muller, F.; Reiser, M.; Sticher, S.; Maier, W.F. The impact of dopants on the activity and selectivity of a Ni-based methanation catalyst. *Appl. Catal. A Gen.* **2009**, *369*, 42–52. [[CrossRef](#)]
29. Feng, S.; Pan, D.; Wang, Z. Facile synthesis of cubic fluorite nano-Ce_{1-x}Zr_xO₂ via hydrothermal crystallization method. *Adv. Powder Technol.* **2011**, *22*, 678–681. [[CrossRef](#)]
30. Xu, S.; Wang, X. Highly active and coking resistant Ni/CeO₂-ZrO₂ catalyst for partial oxidation of methane. *Fuel* **2005**, *84*, 563–567. [[CrossRef](#)]
31. Roh, H.S.; Eum, I.H.; Jeong, D.W. Low temperature steam reforming of methane over Ni-Ce_(1-x)Zr_xO₂ catalysts under severe conditions. *Renew. Energy* **2012**, *42*, 212–216. [[CrossRef](#)]

32. Sánchez-Sánchez, M.C.; Navarro, R.M.; Fierro, J.L.G. Ethanol steam reforming over Ni/M_xO_y-Al₂O₃ (M = Ce, La, Zr and Mg) catalysts: Influence of support on the hydrogen production. *Int. J. Hydrog. Energy* **2010**, *32*, 1462–1471. [[CrossRef](#)]
33. Tan, M.W.; Wang, X.G.; Shang, X.F.; Zou, X.J.; Lu, X.G.; Ding, W.Z. Template-free synthesis of mesoporous γ -alumina-supported Ni-Mg oxides and their catalytic properties for pre-reforming liquefied petroleum gas. *J. Catal.* **2014**, *314*, 117–131. [[CrossRef](#)]
34. Zou, X.J.; Wang, X.G.; Li, L.; Shen, K.; Lu, X.G.; Ding, W.Z. Development of highly effective supported nickel catalysts for pre-reforming of liquefied petroleum gas under low steam to carbon molar ratios. *Int. J. Hydrog. Energy* **2010**, *35*, 13191–13200. [[CrossRef](#)]



© 2017 by the authors. Licensee MDPI, Basel, Switzerland. This article is an open access article distributed under the terms and conditions of the Creative Commons Attribution (CC BY) license (<http://creativecommons.org/licenses/by/4.0/>).